

Super-Resolution Reconstruction of Near-Wall Streak Structures of Turbulent Flows Based on Convolutional Neural Network

*Guoqing Fan, Maokun Ye, Weiwen Zhao, Decheng Wan**

Computational Marine Hydrodynamics Lab (CMHL), School of Naval Architecture, Ocean and Civil Engineering,
Shanghai Jiao Tong University, Shanghai, China

*Corresponding Author

ABSTRACT

Traditional super-resolution convolutional neural network (SRCNN) typically uses the bicubic interpolation results of low-resolution images as input. The size of the feature maps remains unchanged during the training process, which prevents the upsampling process from being effectively learned. In this study, we perform super-resolution reconstruction of near-wall velocity streak by introducing transpose convolution layers to replace interpolation for upsampling in a convolutional neural network. The training data is derived from high-fidelity wall-resolved large eddy simulations (WRLES) of turbulent channel flow at $Re_\tau = 1000$. We specifically focus on the super-resolution performance of present CNN at high ratios ($r = 8, 16$). The results show that the present CNN effectively captures the multi-scale features of wall-bounded turbulence and demonstrates significantly improved training performance compared to the traditional SRCNN, with peak signal-to-noise ratio (PSNR) improvements of 40% and 39.6% for $r = 8$ and $r = 16$, respectively.

KEY WORDS: Super resolution reconstruction; large eddy simulation; near-wall velocity streak; convolutional neural network.

INTRODUCTION

For high Reynolds number wall-bounded turbulence, accurately resolving near-wall coherent structures and capturing small-scale motions requires substantial computational resources, which in turn makes obtaining high-resolution (HR) data exceedingly challenging. Traditional numerical approaches, such as direct numerical simulation (DNS), demand prohibitively fine spatial and temporal resolutions, while experimental methods often fall short of delivering detailed flow field information. In this context, super-resolution (SR) reconstruction methods offer a novel perspective by reconstructing high-resolution flow fields from low-resolution (LR) inputs. SR methods provide a promising direction for alleviating computational challenges and enhancing the accessibility of high-fidelity flow data, thus opening new avenues for turbulence research and engineering applications.

The concept of super-resolution convolutional neural networks (SRCNN) was first introduced by Dong et al. (2016) in their seminal work. This pioneering study demonstrated the capability of deep learning models to reconstruct HR images from LR inputs, marking a significant milestone in the field of image processing. Since its inception, SRCNN and its extensions have been widely adopted in various scientific and engineering domains, including fluid mechanics and turbulence modeling. In the context of near-wall turbulence, recent studies have explored the application of SRCNN-based methods to reconstruct small-scale flow features from coarse-grained simulation or experimental data. The pioneering work by Fukami et al. (2019) introduced machine-learning (ML) based SR methods, utilizing CNN and hybrid downsampled skip-connection/multi-scale models. These methods demonstrated the ability to reconstruct HR turbulent fields, such as two-dimensional cylinder wake and homogeneous isotropic turbulence, from coarse input data with remarkable accuracy. Subsequently, Fukami et al. (2021) extended this approach to spatiotemporal SR reconstruction, integrating temporal dynamics to enhance predictive accuracy in turbulent channel flows. Recent advancements have incorporated novel architectures to further improve reconstruction capabilities. Xu et al. (2023) proposed a transformer-based SR model, leveraging its superior ability to capture long-range dependencies and multiscale features, enabling high-quality reconstruction of isotropic and anisotropic turbulent properties. Similarly, Zeng et al. (2024) developed a hybrid attention framework that effectively integrates multi-dimensional feature fusion, demonstrating its efficacy in reconstructing both laminar and turbulent flows from LR datasets. Sofos et al. (2025) introduced a spatiotemporal SR forecasting model for high-speed turbulent flows, utilizing a lightweight U-Net-inspired architecture to achieve both spatial reconstruction and temporal prediction with low computational overhead.

These investigations have shown promising results, indicating that SR techniques can enhance the representation of near-wall coherent structures while potentially reducing computational demands. Nevertheless, two key challenges remain. First, traditional SRCNN architectures, while effective, are relatively simple and often rely on bicubic interpolation to preprocess LR data, which may limit the model's

ability to fully learn the upsampling process during SR reconstruction. Second, most existing studies have primarily focused on LR data with relatively small downsampling ratios. The effectiveness of SR methods under higher downsampling ratios, where the LR data becomes substantially coarser, remains less explored and warrants further investigation. Addressing these challenges is essential for enhancing the robustness and applicability of SR methods, particularly in scenarios involving highly coarse LR data.

In this study, we perform super-resolution reconstruction of near-wall velocity streak by introducing transpose convolution layers to replace interpolation for upsampling in a convolutional neural network. The training data is derived from high-fidelity WRLES of turbulent channel flow at $Re_\tau = 1000$ (Fan et al., 2024). We specifically focus on the super-resolution performance of present CNN at high ratios ($r = 8, 16$). The results are compared with SRCNN and bicubic. The paper is structured as follows: In Sec. II, we introduce the flow setup of WRLES, data creation for ML training and architecture of present CNN. Sec. III presents the results and detailed discussion. The final conclusions are drawn in Sec. IV.

METHODOLOGY

Governing Equations

The high-fidelity WRLES is based on finite volume method (FVM). By applying a filter to the incompressible N-S equations, the governing equations for LES can be obtained.

$$\frac{\partial \tilde{u}_i}{\partial x_i} = 0, \quad (1)$$

$$\frac{\partial \tilde{u}_i}{\partial t} + \frac{\partial \tilde{u}_i \tilde{u}_j}{\partial x_j} = -\frac{1}{\rho} \frac{\partial \tilde{p}}{\partial x_i} + \nu \frac{\partial^2 \tilde{u}_i}{\partial x_j \partial x_j} + \frac{\partial \tau_{ij}^{sgs}}{\partial x_j}, \quad (2)$$

where \tilde{u}_i ($i = 1, 2, 3$) is the filtered velocity component in the x_i direction of the flow field, \tilde{p} is the filtered pressure of the flow field, ν is the kinematic viscosity of the fluid and τ_{ij}^{sgs} is the SGS stress term. τ_{ij}^{sgs} is given by

$$\tau_{ij}^{sgs} = 2\nu_{sgs} \tilde{\delta}_{ij} + \frac{1}{3} \tau_{kk}^{sgs} \delta_{ij}, \quad (3)$$

where $\tilde{\delta}_{ij}$ is the resolved strain-rate tensor, δ_{ij} is the Kronecker delta, ν_{sgs} is the SGS eddy viscosity. In this study, the wall-adapting local eddy-viscosity (WALE) model (Nicoud and Ducros, 1999) is applied as

$$\nu_{sgs} = (C_w \Delta)^2 \frac{(S_{ij}^d S_{ij}^d)^{\frac{3}{2}}}{(\tilde{S}_{ij}^d \tilde{S}_{ij}^d)^{\frac{3}{2}} + (S_{ij}^d S_{ij}^d)^{\frac{3}{4}}}, \quad (4)$$

where $C_w = 0.325$ is the WALE coefficient, Δ is the cube root of local cell volume, S_{ij}^d is the traceless symmetric part of the square of the velocity gradient tensor.

Flow setup and data creation

Fig. 1 shows the computational domain of WRLES and the size is set to

$L_x \times L_y \times L_z = 2\pi\delta \times 2\delta \times \pi\delta$, where $\delta = 1\text{m}$ is the channel half-height, x , y and z denote the streamwise, wall-normal and spanwise directions, respectively. As for the boundary conditions, periodic boundary conditions are applied in the streamwise and spanwise directions, while a no-slip velocity boundary condition and a zero-gradient pressure condition are prescribed at the top wall and bottom wall. A source term is introduced into the momentum equation to maintain the bulk mean velocity U_b to a constant. The Reynolds numbers based on the bulk velocity and friction velocity are $Re_b = U_b \delta / \nu = 20000$ and $Re_\tau = u_\tau \delta / \nu = 1000$, where $u_\tau = \sqrt{\tau_w / \rho}$ is the friction velocity on the wall.

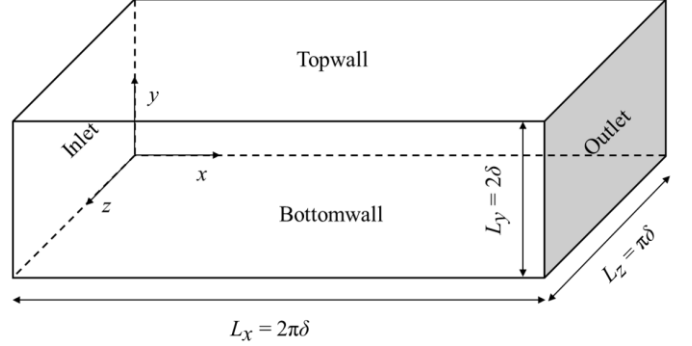


Fig. 1 Computational domain

In terms of the computational meshes, The key parameters of meshes are demonstrated in Table 1, where $N_x \times N_y \times N_z$ are the numbers of grid points in three directions, N_{total} is the total number of grid points, Δx^+ , Δy^+ and Δz^+ are the non-dimensional grid spacings, Δt^+ is the non-dimensional computational time step. In this paper, variables with superscript '+' are non-dimensionalized using characteristic length ν/u_τ and characteristic velocity u_τ . The non-dimensional cell sizes in the wall-normal direction grow gradually from 0.79 at the wall to 15.0 using a linear stretching ratio of 1.05, after which it is uniform. The total number of cells is approximately 22.1 million.

Table 1. Parameters of computational meshes

Case	$N_x \times N_y \times N_z$	Δx^+	Δy^+	Δz^+	Δt^+
WRLES	$321 \times 217 \times 321$	19.6	0.79 ~ 15.0	9.8	0.1

In terms of the numerical schemes and solver, the coupled pressure-velocity is solved using the PISO algorithm (Issa, 1986), with three pressure corrections at each time step. In addition, the temporal term employs the second-order implicit backward scheme (Jasak, 1996). The gradient and Laplacian terms are discretized using the second-order linear scheme. Regarding the discretization of the convective term, the second-order central differencing is used for the convection term in the N-S equations.

Architecture of convolutional neural network

To investigate the effectiveness of SR methods for turbulent flow fields, we employed three CNN architectures. The first network adopts the classic SRCNN architecture, initially proposed by Dong et al. (2016). As shown in Fig. 2(a), the LR data, preprocessed through bicubic interpolation, serves as the input to the SRCNN. The network comprises three convolutional layers with kernel sizes of 9×9 , 5×5 , and 5×5 , respectively. Each layer is followed by a ReLU activation function. The final convolutional layer directly outputs the HR flow field, without applying an activation function, to ensure that the output values remain

consistent with the continuous nature of physical variables.

The second architecture extends the classic SRCNN by increasing the network depth, as illustrated in Fig. 2(b). Additional convolutional layers are introduced to enhance the model's capacity to extract multiscale features from the input data. By deepening the network, this architecture aims to improve the accuracy of high-frequency feature reconstruction, which is critical for capturing the small-scale details of turbulent flows. Similar to the classic SRCNN, the input data is interpolated to the target resolution before being fed into the network. Notably, the size of feature maps of the above two architectures remains constant throughout the network, maintaining the same spatial resolution as the input.

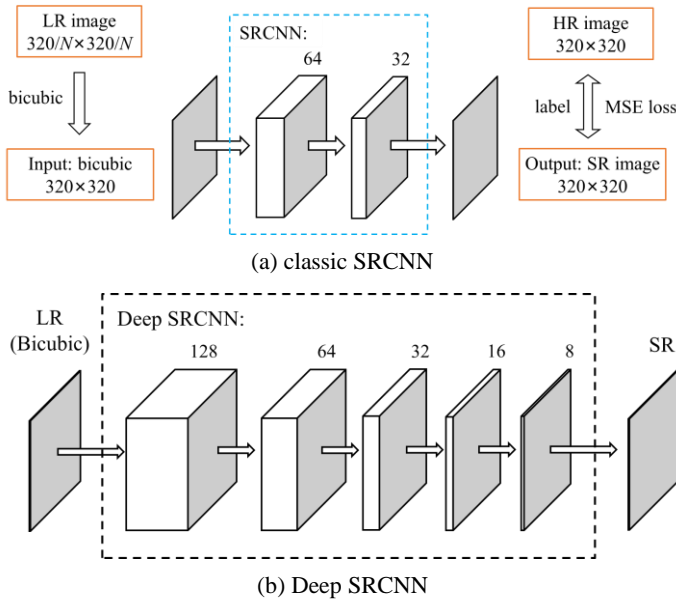


Fig. 2 Architecture of classic SRCNN and deep SRCNN

The third architecture incorporates transposed convolution layers as an explicit upsampling mechanism, replacing the bicubic interpolation step used in the previous architectures. As depicted in Fig. 3, the LR data is directly fed into the network without preprocessing. The transposed convolution layers progressively upscale the input data, enabling the model to learn the upsampling process directly from the training data. The architecture alternates between convolutional layers and transposed convolutional layers, with kernel sizes of 3×3 and 4×4 , respectively. The network architecture in Fig. 3 corresponds to the case with a downsampling ratio of $r = 8$, while for $r = 16$, an additional convolutional layer and transposed convolutional layer are included.

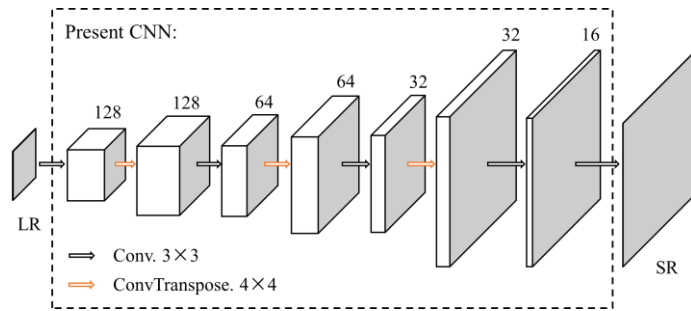


Fig. 3 Architecture of present CNN with transposed convolution layers

The input data consists of LR streamwise velocity fields generated by downsampling HR fields at a specific ratio ($r = 8$ and 16). The

downsampling process discretizes the HR data and the LR data are obtained by selecting discrete points from the HR data. For instance, in the case of $r = 8$, one data point is selected for every eight points. For all architectures, the output is the reconstructed SR flow field, matching the resolution of the original HR data (320×320). During training, the models were optimized using the mean squared error (MSE) loss function, which quantifies the pixel-wise difference between the reconstructed SR image and the ground truth HR data. The Adam optimizer was employed with an initial learning rate of 5×10^{-4} , and we reduced it by $1/5$ when the training loss did not decrease.

RESULTS AND DISCUSSIONS

In this section, we first provide the validation of the training data. Then we present the results of super-resolution reconstruction of turbulent flow fields using different CNN architectures. The study focuses on two downsampling ratios, $r = 8$ and $r = 16$. Considering that the near-wall turbulence is characterized by coherent streak structures and multiscale features, the analysis prioritizes the ability of different models to reconstruct these important characteristics. Quantitative metrics, including loss and Peak Signal-to-Noise Ratio (PSNR) trends during training, are analyzed to assess model performance and provide detailed insights into the reconstruction of near-wall turbulence.

Validation of training data

Fig. 4 shows the instantaneous near-wall vortical structures visualized by the Q -criterion. Due to the approximate symmetry of the channel flow, only the vortex structures from the bottom wall to the center of the channel are presented here. As the distance from the wall increases, the size of the vortices also increases. The multi-scale phenomena of wall-bounded turbulent flow is well observed.

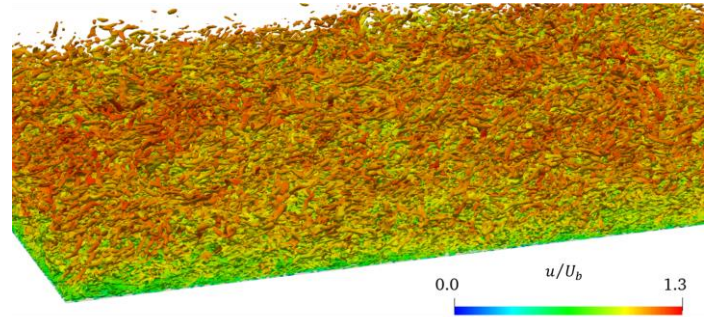


Fig. 4 Instantaneous near-wall vortical structures visualized by the Q -criterion ($Q = 0.05$).

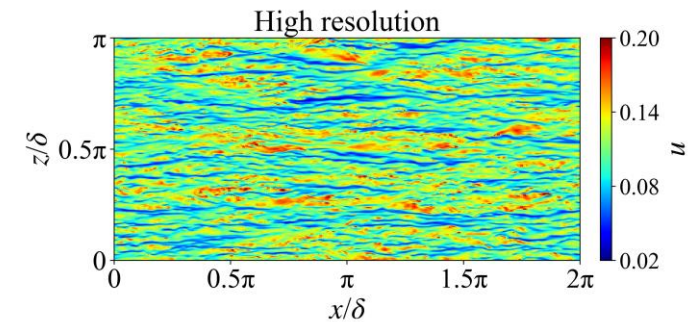
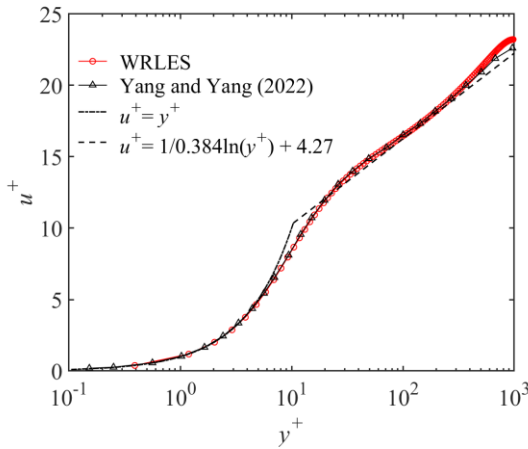


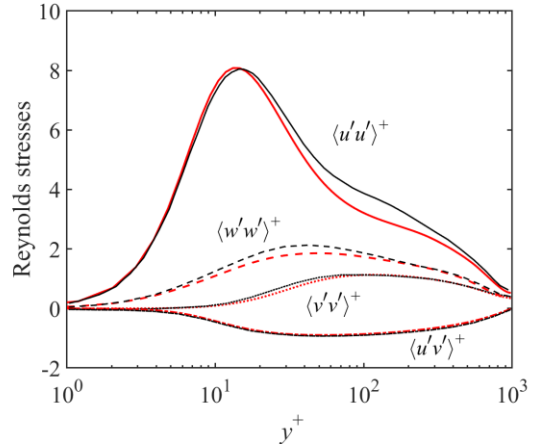
Fig. 5 Instantaneous contours of streamwise velocity fields at $y^+ \approx 15$

Fig. 5 shows the instantaneous contours of streamwise velocity fields (320×320) at $y^+ \approx 15$. The near-wall flow field is organized into streaky quasi-streamwise structures composed of high-speed and low-speed flow. These flows are elongated in the streamwise direction and alternately arranged in the spanwise direction. The low-speed flow primarily originates from the ejection effect, while the high-speed flow results from the sweeping effect of large-scale vortices from above.

Fig. 6 shows the mean streamwise velocity profile and the resolved Reynolds stresses in inner scaling, which are compared with the DNS data (Yang and Yang, 2022). The results of WRLES match well with empirical formulas in both the viscous sublayer and logarithmic layer. For the Reynolds stress $\langle uu \rangle^+$, a peak of Reynolds stress is observed at $y^+ = 15$. The agreement between the DNS data and present WRLES is satisfactory. Considering that $y^+ = 15$ corresponds to the location of the near-wall turbulent kinetic energy peak, where turbulent motions are most active, we chose to perform super-resolution reconstruction on the streamwise velocity field at $y^+ = 15$.



(a) Streamwise velocity profiles



(b) Inner-scaled Reynolds stresses

Fig. 6 Validation of present WRLES. (The red line represents the results of WRLES, the black line shows the DNS data.)

Results for downsampling rate $r = 8$

Fig. 7 display the LR input, bicubic interpolation, HR target flow fields, and the reconstructed near-wall streak under different neural network at $r = 8$. The LR input exhibits a coarse representation of the near-wall flow field. Bicubic interpolation improves spatial resolution to some extent but introduces smoothing effects that obscure the streak structures and fail to capture their dynamic characteristics. In contrast, the HR flow field resolves these streak structures in detail, providing an accurate reference for evaluating SR performance.

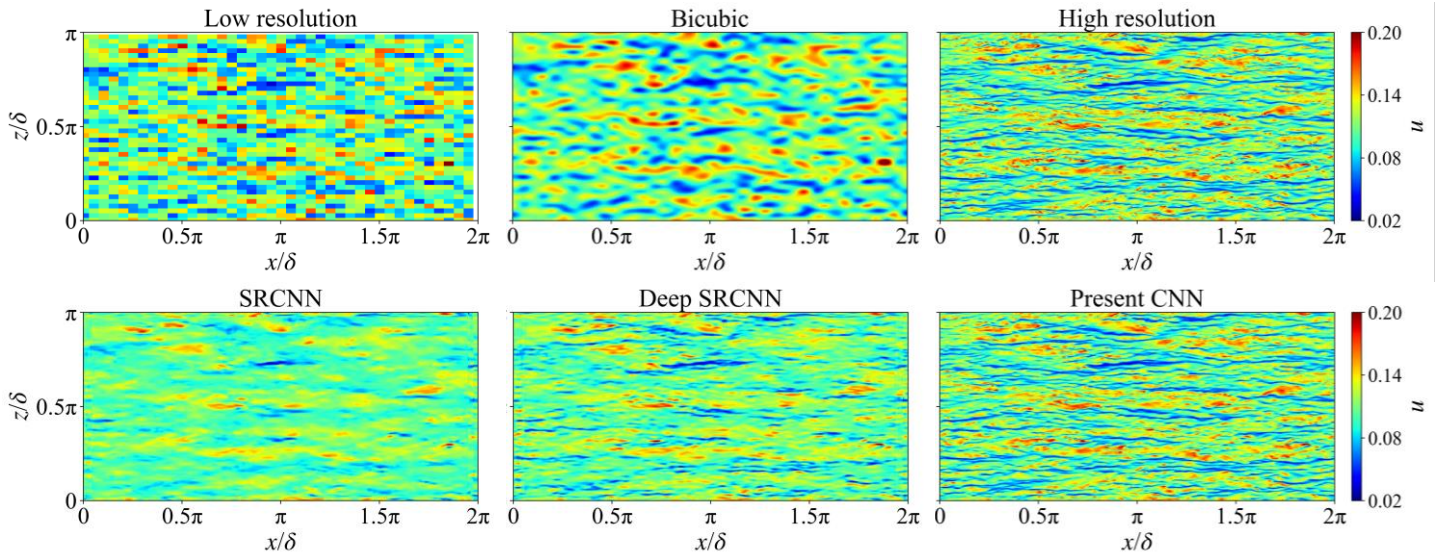


Fig. 7 Reconstructed near-wall streak under different neural network at $r = 8$.

In terms of the reconstructed results, the SRCNN (Dong et al., 2016) partially recover large-scale features but fail to capture the coherence and small-scale details of the streak structures. The deep SRCNN

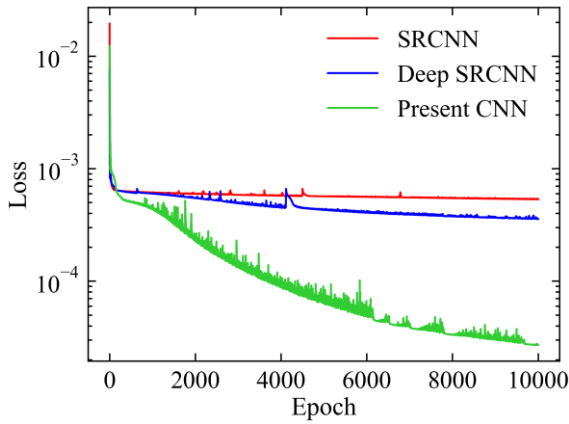
architecture enhances the representation of multiscale features, showing better alignment with the streak structures compared to SRCNN. The present CNN architecture, incorporating transposed convolution,

exhibits the best reconstruction performance. The present CNN, incorporating transposed convolution layers, provides the most accurate reconstruction. It effectively resolves the anisotropic and multiscale features of near-wall turbulence, restoring both the coherence and small-scale fluctuations of the streaks.

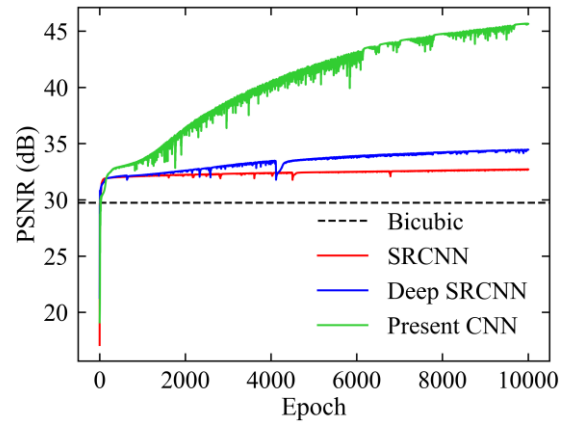
Fig. 8 presents the loss and PSNR trends during training for $r = 8$. The definition of PSNR is given as:

$$\text{PSNR} = 10 \cdot \log_{10} \left(\frac{\text{MAX}_1^2}{\text{MSE}} \right) = 20 \cdot \log_{10} \left(\frac{\text{MAX}_1}{\sqrt{\text{MSE}}} \right), \quad (5)$$

where, MAX_1 represents the maximum pixel value of the image, and the unit of PSNR is dB. The loss curves shown in Fig. 8(a) indicate that the present CNN achieves the lowest final loss, reflecting its superior ability to minimize reconstruction errors. Notably, the SRCNN exhibits signs of gradient vanishing, as evidenced by its slower convergence and higher final loss values. The PSNR trends in Fig. 8(b) further confirm this observation, with the present CNN achieving a final PSNR of 45 dB, representing a 40% improvement over SRCNN's 32 dB and a 32% improvement over Deep SRCNN's 34 dB. The incorporation of transposed convolution layers allows the model to directly learn the upsampling process, contributing to its higher accuracy in capturing streak structures.



(a) Training loss



(b) PSNR

Fig. 8 Training loss and PSNR trends of three architectures at $r = 8$

Results for downsampling rate $r = 16$

Figures 9 display the reconstructed near-wall streak under different neural network $r = 16$. The LR input represents an even coarser flow field compared to $r = 8$, where the streak structures are almost completely lost. Bicubic interpolation provides minimal improvement, with the streak structures remaining indistinguishable. Fig. 9 also presents the reconstructed flow fields using the SRCNN, deep SRCNN, and present CNN architectures. The SRCNN results offer limited improvement over bicubic interpolation, failing to recover the streak structures. The Deep SRCNN performs better, reconstructing some large-scale features but still lacking in the resolution of small-scale fluctuations. The present CNN architecture, however, demonstrates superior performance. It accurately reconstructs the streak structures near the wall, recovering their elongated and coherent characteristics, even under the challenging $r = 16$ condition. This highlights the robustness of the present CNN architecture in learning complex anisotropic features from highly coarse input data.

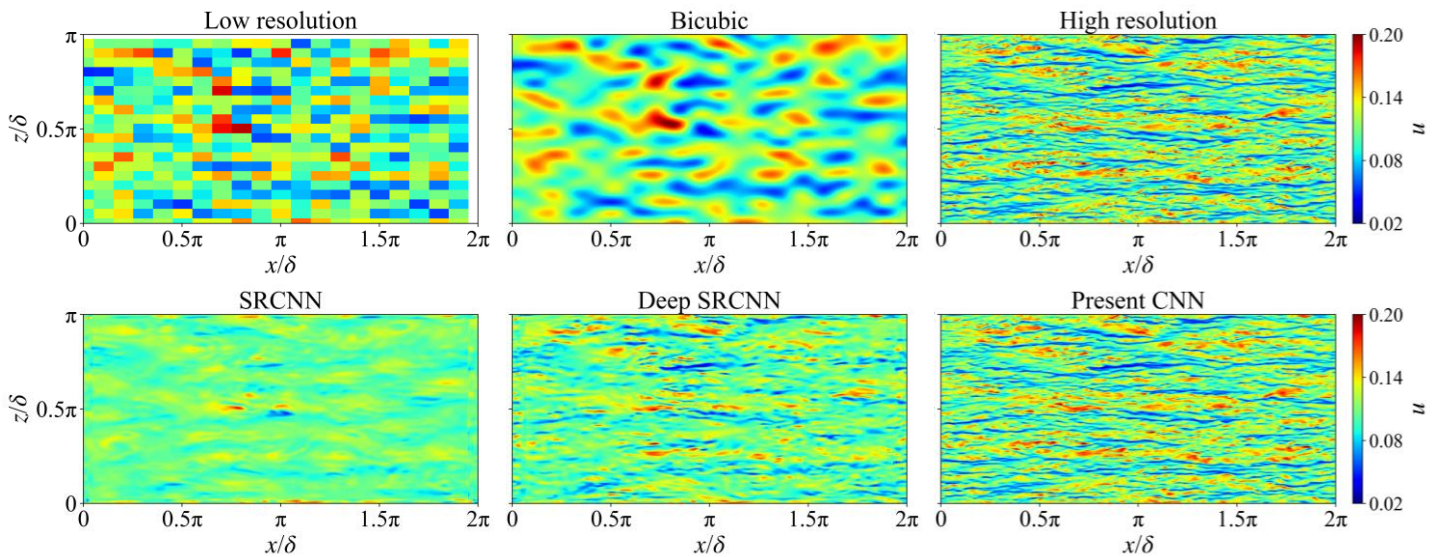


Fig. 9 Reconstructed near-wall streak under different neural network at $r = 16$.

Figure 10 shows the loss and PSNR trends during training for $r = 16$. The loss curves reveal that all models converge to stable values, but the present CNN achieves the lowest final loss, significantly outperforming the other architectures. Similarly, the PSNR trends show that the present CNN reaches a final PSNR of 44 dB, indicating a 39.6% improvement over SRCNN's 31.5 dB and a 31.3% improvement over Deep SRCNN's 33.5 dB. The results highlight the effectiveness of the transposed convolution layers in learning the upsampling process for highly coarse input data.

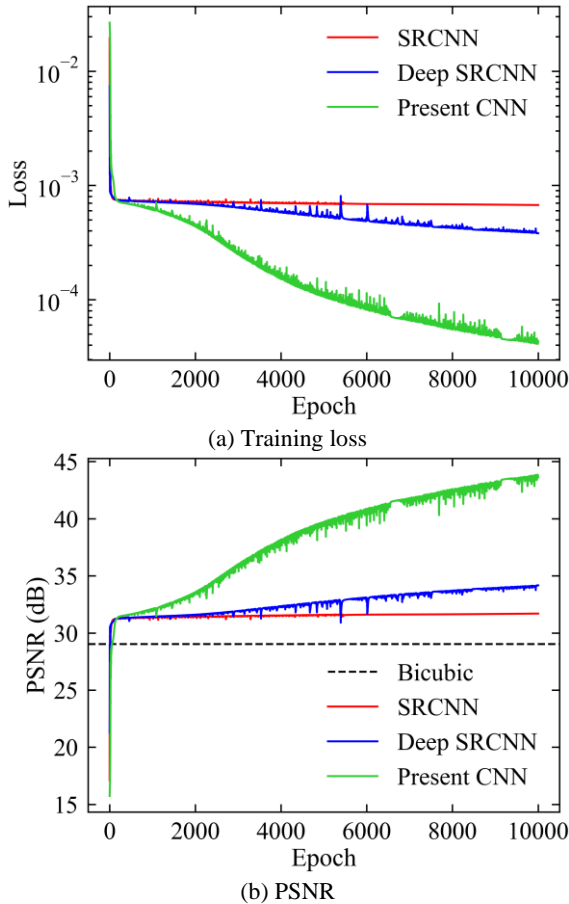


Fig. 10 Training loss and PSNR trends of three architectures at $r = 16$

The comparisons between $r = 8$ and $r = 16$ highlight the increasing challenges of reconstructing near-wall turbulent streak structures as the downsampling ratio grows. While all models exhibit some performance degradation with coarser input data, the present CNN consistently outperforms the SRCNN and deep SRCNN architectures. Notably, in both SRCNN and deep SRCNN architectures, the feature map dimensions remain constant during training, but the number of channels decreases progressively. This reduction likely leads to information loss during neural network propagation, resulting in poorer training outcomes, especially at higher downsampling ratios. In SR reconstruction tasks, which essentially involve upsampling, the first two architectures delegate the upsampling process to bicubic interpolation. In contrast, the present CNN architecture incorporates transposed convolution layers, allowing the neural network to learn the upsampling process directly, leading to better training performance. These findings underscore the potential of the present CNN architecture for applications requiring high-fidelity reconstructions of near-wall turbulence in engineering and scientific contexts.

CONCLUSIONS

In this study, we perform super-resolution reconstruction of near-wall velocity streak by introducing transpose convolution layers to replace bicubic for upsampling in the convolutional neural network. The training data is derived from high-fidelity WRLES of turbulent channel flow at $Re_\tau = 1000$ (Fan et al., 2024). We specifically focus on the super-resolution performance of present CNN at high ratios ($r = 8, 16$). The results demonstrate the significant potential of SR techniques in recovering critical features of near-wall turbulence, such as coherent streak structures and multiscale dynamics, even under substantial data degradation.

The findings highlight the limitations of traditional SRCNN and Deep SRCNN architectures. These models rely on bicubic interpolation for upsampling, which bypasses the network's ability to learn this critical process, resulting in information loss, particularly as feature map channels are progressively reduced during training. This limitation is especially evident at higher downsampling ratios, where the reconstruction of fine-scale and anisotropic features becomes increasingly challenging.

In contrast, the present CNN architecture incorporates transposed convolution layers, enabling the network to directly learn the upsampling process. This design effectively addresses the challenges associated with large downsampling ratios, achieving higher PSNR values and demonstrating superior reconstruction accuracy. The present CNN successfully captures both the spatial coherence and intermittent small-scale fluctuations of near-wall turbulent streak structures, showcasing its robustness and scalability.

Overall, this study establishes the feasibility of using SR methods, particularly the present CNN architecture, to address the challenges posed by high-resolution reconstruction of turbulent flows. Future work could extend this approach to testing datasets, explore generalization to diverse flow scenarios, and investigate further optimization of network architectures for turbulence modeling and engineering applications. Additionally, since the current LR flow field data are obtained by downsampling from HR data, it is challenging to acquire paired high-resolution and low-resolution data from actual CFD simulations for training. Future work could further explore the incorporation of unsupervised learning architectures, including cycle generative adversarial networks (cycleGANs), to address this issue.

ACKNOWLEDGEMENTS

This work is supported by the National Natural Science Foundation of China (52131102), to which the authors are most grateful.

REFERENCES

- Dong, C, Loy, CC, He, K, and Tang, X (2016). "Image super-resolution using deep convolutional networks," *IEEE Trans Pattern Anal Mach Intell*, 38(2), 295–307.
- Fan, GQ, Zhu, J, Zhao, WW, and Wan, DC (2024). "A comparative study between wall-resolved and wall-modeled large eddy simulation of turbulent channel flows," *34th International Ocean and Polar Engineering Conference*, Rhodes, Greece, OnePetro, 220–226.
- Fukami, K, Fukagata, K, and Taira, K (2019). "Super-resolution reconstruction of turbulent flows with machine learning," *J Fluid Mech*, 870, 106–120.

- Fukami, K, Fukagata, K, and Taira, K (2021). "Machine-learning-based spatio-temporal super resolution reconstruction of turbulent flows," *J Fluid Mech*, 909, A9.
- Issa, RI (1986). "Solution of the implicitly discretised fluid flow equations by operator-splitting," *J Comput Phys*, 62(1), 40–65.
- Jasak, H (1996). "Error analysis and estimation for the finite volume method with applications to fluid flows," PhD thesis. Imperial College, University of London.
- Nicoud, F, and Ducros, F (1999). "Subgrid-scale stress modelling based on the square of the velocity gradient tensor," *Flow Turbul Combust*, 62, 183–200.
- Sofos, F, Drikakis, D, Kokkinakis, IW, and Spottswood, SM (2025). "Spatiotemporal super-resolution forecasting of high-speed turbulent flows," *Phys Fluids*, 37(1), 016124.
- Xu, Q, Zhuang, Z, Pan, Y, and Wen, B (2023). "Super-resolution reconstruction of turbulent flows with a transformer-based deep learning framework," *Phys Fluids*, 35(5), 055130.
- Yang, BW, and Yang, ZX (2022). "On the wavenumber-frequency spectrum of the wall pressure fluctuations in turbulent channel flow," *J Fluid Mech*, 937, A39.
- Zeng, K, Zhang, Y, Xu, H, and Feng, XL (2024). "Super-resolution reconstruction of turbulent flows with a hybrid framework of attention," *Phys Fluids*, 36(6), 065107.